JCTC Journal of Chemical Theory and Computation

Pressure Annealing as a Complement to Temperature Annealing To Find Low-Energy Structures of Oligomeric Molecules

Christopher Adam Hixson and Ralph A. Wheeler*

Department of Chemistry and Biochemistry, University of Oklahoma, 620 Parrington Oval, Room 208, Norman, Oklahoma 73019

Received October 27, 2008

Abstract: Finding the lowest-energy geometry of a molecule or collection of molecules is a fundamental challenge of modern computational chemistry and is closely related to the more general problem of optimizing a function. Temperature annealing, popularly called simulated annealing, is a powerful and commonly used technique, but it is not well suited to conformational sampling of long, oligomeric molecules. A method is presented herein that incorporates pressure as an optimization parameter to complement temperature annealing, and several tests of its effectiveness are described. Bayesian statistical analysis shows that pressure−temperature annealing confers no advantage in control simulations of Lennard-Jones particles, but it yields lower-energy structures than pure temperature annealing with significant credibility for two model polyethers, monoglyme ($CH_3OCH_2CH_2OCH_3$) and tetraglyme [$CH_3(OCH_2CH_2)_4OCH_3$].

1. Introduction

Polymers or long-chain molecules designed to model polymers are generally difficult candidates for computational study because their multiple conformations make it difficult to find low-energy structures. This manifests as a glassy potential energy surface that complicates application of computational methods[1] typically employed in studying the structural and thermodynamic properties of these systems such as molecular dynamics (MD) or Monte Carlo (MC) methods.[2] Generally, MD and MC computations are supplemented by techniques such as simulated (temperature) annealing to improve the quality of the results.[3−9] This is especially true in structural studies, particularly when searching for low-energy states of such systems.[6−8] Alternative methods are available and are commonly used,[10,11] as no one class of optimization methods is suited to all problems. A technique is presented here that expands temperature annealing by using pressure as an additional control parameter. This extra parameter is tested to assess its utility in the special case of frustrated, glassy systems. First, we review optimization techniques employed in the study of complex systems, such as those studied here. Then, we explain the advantages of the temperature annealing approach and show how the addition of pressure as a parameter modifies the method. Finally, we present statistical analyses that demonstrate the value of our proposed approach.

1.1. Popular Molecular-Dynamics-Based Optimization Methods. One of the most important pieces of information useful to understanding chemical phenomena is structure. Understanding the spatial arrangement of the atoms contained in a chemical system might seem rather basic, but it is necessary to provide insights into the thermodynamics, reactivity, and spectroscopic properties of the system. Of course, determining the structure of chemical systems can be accomplished experimentally using X-ray crystallography,[12] NMR spectroscopy,[13] and other methods.[14] Quite commonly now, structural models are proposed based on computational studies. Using the quantum approach,[15] structures of small or even medium-sized molecules are routinely determined to great accuracy. For larger systems, including condensed-phase structures, accuracy is traded for computational efficiency, and molecular mechanics methods are employed.[16] Molecular mechanics methods take, for example, the AMBER force field[17] and use optimization methods traditionally used in mathematics, such as the conjugate gradient algorithm,[18] to find minima of the energy

* Corresponding author e-mail: rawheeler@ou.edu.

10.1021/ct800451c CCC: $40.75
Published on Web 05/22/2009

function. This is a useful approach, but it has limited utility for a variety of reasons, including limiting the search to finding local minima "near" the starting structure. More commonly used is molecular dynamics or Monte Carlo,[2] coupled with some optimization algorithm. Some popular algorithms, including temperature annealing (usually called simulated annealing),[4] a popular algorithm fundamentally important to this contribution, are discussed below.

1.1.1. Locally Enhanced Sampling. Locally enhanced sampling (LES)[19] is a technique that was first proposed in 1990 (the original idea was taken from another method)[20] and was initially designed to improve the search for diffusion paths of small ligands inside a protein matrix. It has since become a moderately popular optimization method, useful when the structure of a small part of the system is needed in relation to the remainder. This small part of the system is copied several times. None of the copies directly interacts with the others, but instead, each one interacts directly with the remainder of the system, generally referred to as the bath. Atoms in the bath interact normally with each other, but they interact with the average of each of the copied systems. It is often claimed that this algorithm allows the interaction between the copied parts of the system and the bath to be smoothed. Specifically, it has been reported that any barriers resulting from this interaction would be decreased proportionally to the number of times the smaller part of the system was copied.[21] Individual copies frequently gain energy during the simulation, allowing for a sort of "tunneling" behavior. Thus, each copy can be given a greater allotment of energy than in traditional molecular dynamics, and so can better explore the potential energy surface, until the energy is redistributed to the other systems via the bath interaction.[22]

The method has been used to explore potential energy surfaces in several situations.[11,21,23−26] The trajectory mapping application used in the original article is an important example, and there have been other applications of LES to finding low-energy structures.[11,21,23−26] Although not as commonly used as the method described in the next section, LES is still a relatively popular method and has been implemented in a variety of molecular dynamics packages in common use.

1.1.2. Replica Exchange. The replica-exchange molecular dynamics simulation method is quite popular. First proposed in 1999,[10] the method has a relatively straightforward implementation. The entire system under study is replicated a number of times. Each replica is independent and is held at a different temperature, with the set of replicas spanning a range of temperatures. The systems are allowed to evolve using molecular dynamics for a set number of time steps, and then, the temperatures of two systems are exchanged if they pass a Metropolis test. Because the probability of acceptance is low if the temperatures vary too much, only exchanges between systems of neighboring temperatures are typically attempted.

Generally described as finding minima on the free energy surface, replica exchange has been used to study a variety of systems, including polypeptides, proteins, and polymers.[10,27−32] The method has shown great utility in mapping low-energy structures of peptide systems, although many other examples can be found in the literature. This method owes a large part of its existence to temperature annealing, as the methods are quite similar in approach, although temperature annealing has been in use for a much longer time.

1.2. Temperature Annealing. The idea that a state having a given energy is populated with a calculable relative probability is one of the most fundamental ideas in statistical physics and is immortalized (at least for the canonical ensemble) in the Boltzmann distribution. Given this link between such a readily obtainable quantity (the energy) and relative population, it should come as no surprise that an optimization strategy, temperature annealing, would be formed from it. Simply put, temperature annealing[4] is a process in which an ensemble of states of a system is generated corresponding to high-energy conditions (by raising the temperature) and the system is allowed to evolve toward a lower-energy state. As cooler states are generated, the system tends to settle into areas of low energy, because, at lower temperatures, these areas are more likely to be populated. Raising the temperature initially widens the search area by increasing the volume of phase space available to be populated because the systems have a greater probability of surmounting barriers separating regions of phase space. Then, lowering the temperature traps the system in wells with a probability that depends on their energy and phase-space volume.

One surprising aspect of temperature annealing is that, despite its specific link to statistical physics, it has shown its worth in a variety of fields as a general-purpose optimization technique.[4] Such general use can be contemplated because a wide variety of problems exist that allow a cost function analogous to the energy to be defined. In one famous example, the traveling salesman problem, the object is to find the quickest path connecting two points along some complicated linkage structure sharing features found in road maps. The energy is represented by a cost function generally chosen to be a function of the number of nodes the salesman must cross. This function is optimized, generally, using a Monte Carlo procedure where each newly generated state is compared with the previous one and either accepted or rejected according to the Metropolis criterion.[2] The temperature is a fictitious parameter, but by increasing it, the algorithm accepts trial moves with a greater frequency, thereby allowing states of higher "energy" to be visited. Lowering the temperature biases the simulation into lower-energy states. This behavior is exactly analogous to the role of temperature in condensed-phase systems. Similar methods have been used to solve problems in electrical engineering to design circuits and in signal processing to process images and sounds.[4] Finally, the most traditional area of application is in finding energy minima in condensed systems either by using the Metropolis/Monte Carlo method outlined above or by using molecular dynamics as the ensemble-generation engine.[2]

1.3. Role of Pressure. Complementing temperature annealing with pressure annealing to locate low-energy geometries more quickly has the potential of improving the quality of temperature annealing searches. As described above, one

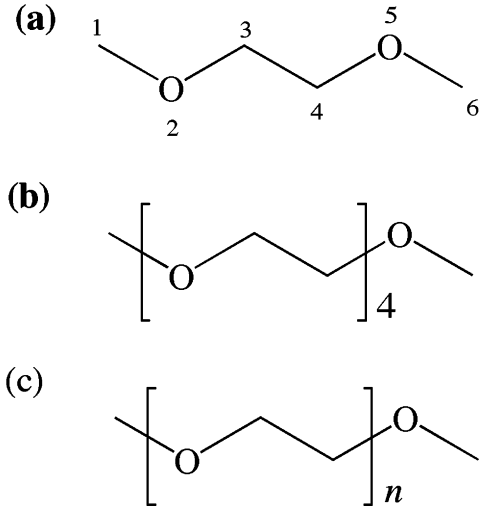

Figure 1. Structures of the oligomeric models used in this work: (a) monoglyme and (b) tetraglyme. These structures are oligomeric models of (c) the polymer polyethylene oxide.

role of temperature is to help define the phase-space area to search in a temperature annealing optimization. If the system is located in an area of phase space separated cleanly from another by a large barrier, the separated area will only rarely be visited within the calculation. This situation requires a particularly long simulation to obtain an accurate result. As the temperature is raised ever higher, the structure becomes more likely to surmount such a barrier; however, raising the temperature can become counterproductive by causing the simulation to become unstable or increasing the simulation time. Consequently, making more sensible changes to other simulation variables such as pressure is an avenue worth exploring. Adjusting the pressure indirectly affects the optimization because the pressure determines the volume (and thus the density) of the system, which, in turn, affects the amount of phase space available to be explored. It increases the fraction of explorable phase space by a different approach than using temperature alone. The effects of such changes are explored below.

1.4. Objectives of This Work. Several systems are tested here to illustrate the benefits that using pressure as an optimization control parameter can add to a temperature annealing optimization strategy. First, the method is tested on a system composed of Lennard-Jones particles.[33] This system is relatively simple and is used here are a control. Because the glassy nature of their energy surfaces makes conformational trapping a serious issue,[1] simulations of polymers and polymer models are expected to benefit greatly from pressure annealing. Thus, we also test two models for the polymer polyethylene oxide (PEO)[34−36] called monoglyme and tetraglyme (see Figure 1). PEO is interesting for several applications, including use as the matrix for polymer-ion batteries.[37,38] Monoglyme is an oligomer containing one unit of the PEO polymer, tetraglyme contains four units, and both of these systems have previously been studied.[34−36]

2. Statistical Mechanical Basis of Pressure Annealing

Temperature annealing is among the most frequently used optimization methods in chemistry for a variety of reasons. First, the method makes a great deal of intuitive sense and can be explained almost entirely using basic appeals to logic. On the other hand, temperature annealing has been formally proven to be an optimization technique and is on a firm mathematical basis.[5,39] It has even been shown that, when a proper cooling schedule is used, the method is guaranteed to find the global minimum of the system.[39] Although, in practice, the conditions required to realize the promise of temperature annealing are impossible to achieve completely, the fact that the method could, in principle, attain success is quite appealing. Perhaps this combination of being easily understood, effective, and firmly rooted in theory explains why temperature annealing is one of the most popular optimization methods in use, not only in chemistry, but also in a wide variety of other fields. What follows is an abridged summary of temperature annealing, to substantiate the pressure−temperature annealing procedure proposed in this work.

2.1. Temperature Annealing. A simple, qualitative way of explaining why temperature annealing works starts by noting that low-temperature states corresponding to low energies should be populated with greater probability than higher-energy states, whereas at higher temperatures, the populations are less strictly related to the energy of the state. This is due to the flattening of the probability distribution observed at higher temperatures. In the high-temperature phase of the optimization, the system wanders and explores phase space with relatively lax restrictions and freezes into the states of higher probability at lower temperatures. It has been proven that repeated application of heating−cooling cycles is guaranteed eventually to find the lowest-energy states.[5,39] It is also instructive to note that temperature annealing finds the minimum of the energy E by manipulating the parameter β in the expression

$$Q(N, V, T) = \frac{1}{C}\int_{-\infty}^{\infty} \mathrm{e}^{-\beta E}\Omega(N, V, E)\,\mathrm{d}E$$

where T is the temperature (β is the inverse of the product of the temperature and the Boltzmann constant), V is the volume, C is a normalization constant, and N is the number of particles. Q is the canonical partition function, and Ω is the microcanonical partition function. In this framework, simulated annealing can be interpreted as finding the lowest energy for a system containing N particles in a volume V.

2.2. Pressure Annealing. To understand how pressure can be used as an optimization variable, consider an expression similar to the canonical ensemble partition function written above, but for a related ensemble. Because the pressure divided by the temperature is conjugate to the volume,[40] we know that if βp (where p is the pressure of the system) is fixed, thus allowing the volume to fluctuate, we can write a partition function for that ensemble as

$$M(N, \beta p, E) = \frac{1}{C}\int_{0}^{\infty} \mathrm{e}^{-\beta pV}\Omega(N, V, E)\,\mathrm{d}V$$

All of the variables are the same as described in the previous section, and M is the partition function for the *NPE* ensemble. This expression for the partition function is reasonable given that $\Omega \sim V^N$ is weighted by $e^{-\beta pV}$ as V gets large. It is also apparent that, as the pressure increases, the volume decreases. Conversely, decreasing the volume increases pressure. When the pressure vanishes, the volume becomes unbounded. By manipulating βp as the temperature was manipulated in temperature annealing, the function V is minimized. This can be interpreted as finding the smallest volume able to contain N particles with an energy E and implies that pressure annealing alone is unlikely to prove effective as an energy optimization strategy.

2.3. Benefit to Including Pressure in Simulated Annealing Optimizations. In the isothermal−isobaric ensemble (*NPT*), pressure and temperature are fixed in the partition function. Using this knowledge, we constructed an optimization strategy to take advantage of pressure as a parameter alongside temperature in a pressure−temperature simulated annealing strategy. From the analysis in the previous two sections, it is clear that using pressure as an optimization parameter does not act to optimize the energy; however, the pressure does control features of a simulation that can be exploited to aid in simulated annealing. If the pressure is fixed at a small value, the density of the system decreases as the volume of the system increases. For some systems, this is not particularly helpful for optimization, but for bulky systems where geometry changes are hindered at the density of interest, increasing the available volume can be quite helpful. By allowing the molecules to separate, intramolecular energies can be minimized more easily. Then, by increasing the pressure, the molecules can be compressed efficiently into a low-energy state, optimizing the volume using the procedure explained in the previous section. Using these principles, pressure−temperature simulated annealing strategies can be designed. The strategy presented here consists of four steps. The first step allows an expansion to occur from the initial state by fixing the temperature and pressure at low values. After the expansion, the volume is fixed, and traditional temperature annealing is performed on the expanded system. Third, after temperature annealing is completed, the pressure is fixed to a large value, and the temperature remains fixed at the final annealing temperature. Finally, after the compression, the system's energy is minimized. The totality of the method allows two complications of temperature annealing to be addressed. First, in condensed-phase systems of molecules with hindered rotations, inducing intramolecular conformational changes can be difficult. This can also lead to difficulty in changing the way the system packs.

Understanding how lowered density might benefit a simulation is not difficult. Imagine the simple two-dimensional system depicted in Figure 2. This system consists of a string of eight beads connected to each other in a coil by springs of length r. The beads do not interact except through the springs and can be considered hard spheres. The entire coil is contained in a box with sides of length L. If an optimization algorithm seeks to characterize the low-energy states of this system, moving from the counterclockwise coil depicted in the figure to the clockwise coil would be an important transition. The height of the lowest barrier between these two states determines the difficulty of making the transition. If the length of the box is $8r$ or greater, no barrier to the transition exists because the system can align as a

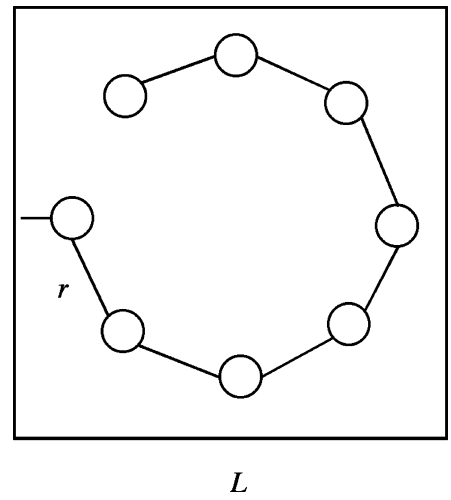

Figure 2. Simple two-dimensional model representing a coiled molecule. The molecule exists inside a box whose walls are treated as large potential energy barriers, each side of which has length L. The molecule is composed of beads connected by springs, whose equilibrium length is r. When the length of the side of the box is greater than $7r$, the molecule can change coil orientation without needing to surmount any barrier, illustrating that increasing the available volume can make conformational searches easier.

Table 1. Final Energies (kcal mol^{-1}) Determined by Temperature Annealing and Pressure−Temperature Annealing Algorithms for Each of the 50 Lennard-Jones Systems Studied[a]

system	temperature annealing	pressure−temperature annealing	system	temperature annealing	pressure−temperature annealing
1	−953.54	−959.72	26	−955.89	−954.60
2	−955.53	−958.15	27	−954.38	−957.08
3	−951.82	−941.17	28	−957.22	−957.02
4	−963.88	−958.96	29	−955.10	−964.38
5	−959.86	−957.37	30	−953.17	−954.55
6	−955.72	−962.54	31	−953.00	−954.04
7	−958.82	−960.63	32	−953.45	−953.38
8	−958.23	−952.44	33	−942.91	−955.55
9	−957.33	−957.85	34	−956.65	−949.70
10	−952.84	−955.26	35	−955.83	−955.21
11	−960.52	−958.35	36	−957.34	−959.68
12	−944.61	−951.79	37	−960.03	−959.50
13	−955.15	−957.99	38	−956.19	−948.28
14	−960.71	−947.03	39	−957.45	−960.63
15	−956.07	−951.94	40	−961.74	−956.73
16	−955.63	−960.72	41	−952.40	−962.08
17	−960.70	−953.16	42	−953.11	−961.18
18	−958.62	−956.65	43	−958.97	−960.29
19	−956.99	−957.29	44	−959.52	−961.30
20	−959.05	−953.37	45	−959.73	−959.84
21	−959.97	−956.79	46	−952.60	−958.94
22	−957.59	−955.11	47	−945.38	−958.56
23	−957.30	−954.24	48	−953.92	−963.10
24	−960.38	−945.11	49	−953.77	−956.70
25	−958.37	−952.55	50	−958.79	−955.04

[a] Each pair of simulations started from the same randomly generated initial structure. Neither method seems to be superior to the other, as the lowest energy was found with equal likelihood by the two methods.

Table 2. Final Energies (kcal mol^{-1}) Determined by Temperature Annealing and Pressure−Temperature Annealing Algorithms for Each of the 25 Monoglyme Systems[a]

system	temperature annealing	pressure−temperature annealing
1	−734.8209	−741.6008
2	−722.3525	−741.6008
3	−721.0294	−741.6008
4	−735.0073	−741.6008
5	−737.5804	−741.6008
6	−729.8086	−741.6008
7	−728.0307	−741.6008
8	−741.7752	−741.6008
9	−727.7178	−741.6008
10	−730.5577	−741.6008
11	−729.5520	−736.1320
12	−729.5520	−737.8802
13	−729.5520	−738.9512
14	−729.5520	−740.6107
15	−729.5520	−725.5618
16	−729.5520	−734.7025
17	−729.5520	−717.1497
18	−729.5520	−732.1472
19	−729.5520	−733.4708
20	−729.5520	−741.2944
21	−744.3963	−715.6028
22	−737.9864	−751.5224
23	−719.8457	−742.0861
24	−734.7466	−737.3870
25	−728.8936	−733.7409

[a] Each pair of simulations started from the same randomly generated initial structure. The pressure−temperature annealing algorithm preferentially gave the lowest energy approximately 80% of the time.

straight line while maintaining each of the springs at its equilibrium length. If the box is smaller than the radius of the semicircle, the system cannot make the transition to the low-energy state. Systems complicated enough to be of chemical interest must account not only for this constraint, but also for different packing arrangements. Both are dealt with by the pressure annealing procedure. Choosing the details of pressure annealing simulations with these facts in mind are important to a successful simulation.

3. Model Systems and Procedure

Several systems were used to compare pressure annealing with temperature annealing. These systems range from a relatively simple model Lennard-Jones system to oligomeric models of polyethylene oxide. In each case, two sets of simulations were performed. First, traditional temperature annealing was performed. In these simulations, the system was elevated in temperature starting from 25 to 1025 K over the course of a simulation on the nanosecond time scale. After the temperature annealing simulation, the system was further minimized using a conjugate gradient method. The minimized structure and energy were reported. Second, pressure−temperature annealing was performed. These simulations can be divided into three distinct steps. The first step involves heating while allowing the system to expand slowly. The second phase allows the system to expand dramatically while maintaining the hottest temperature of the initial annealing cycle. Finally, the system is compressed to its original volume while being cooled. The system is then subjected to the same minimization procedure as in the simulated annealing simulation, and the final minimized structure and energy are reported.

Table 3. Final Energies (kcal mol^{-1}) Determined by Temperature Annealing and Pressure−Temperature Annealing Algorithms for Each of the 25 Tetraglyme Systems[a]

system	temperature annealing	pressure−temperature annealing
1	−105.0748	−103.9599
2	−98.6349	−99.8905
3	−100.5817	−107.2664
4	−105.0766	−105.9834
5	−106.7726	−98.3929
6	−102.2849	−101.1396
7	−114.2732	−102.1396
8	−107.0713	−107.6627
9	−105.9728	−107.8258
10	−98.4871	−100.2481
11	−81.9171	−91.4357
12	−118.1657	−107.4743
13	−91.2899	−98.9836
14	−96.3824	−124.9147
15	−83.3597	−110.0198
16	−100.6137	−116.6695
17	−110.3598	−101.1773
18	−87.3115	−108.4409
19	−101.0185	−113.5207
20	−103.8985	−109.7915
21	−94.2803	−108.7402
22	−89.5132	−94.8436
23	−108.8482	−100.1544
24	−87.5746	−96.8615
25	−97.6049	−94.4017

[a] Each pair of simulations started from the same randomly generated initial structure. The pressure−temperature annealing algorithm preferentially gave the lowest energy approximately 70% of the time.

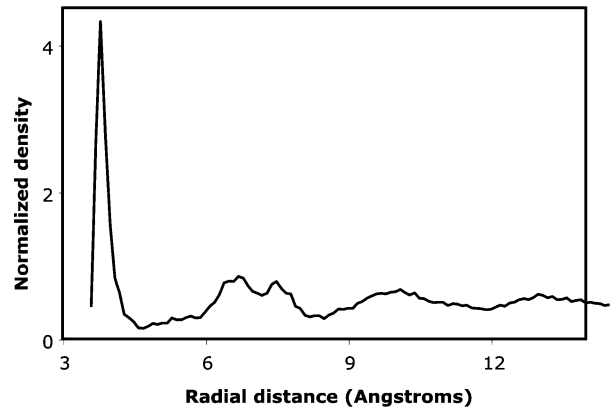

Figure 3. Radial distribution function formed from the data taken from the lowest-energy structure found in the Lennard-Jones simulations. It is representative of our results and compares well with previously obtained results.

3.1. Particles with Only Lennard-Jones Interactions. This model system contained particles of argon with a mass of 40 amu. Here, the force between the particles is the (12,6) Lennard-Jones model for van der Waals forces, written as

$$V(r) = 4\varepsilon\left(\frac{\sigma^{12}}{r^{12}} - \frac{\sigma^{6}}{r^{6}}\right)$$

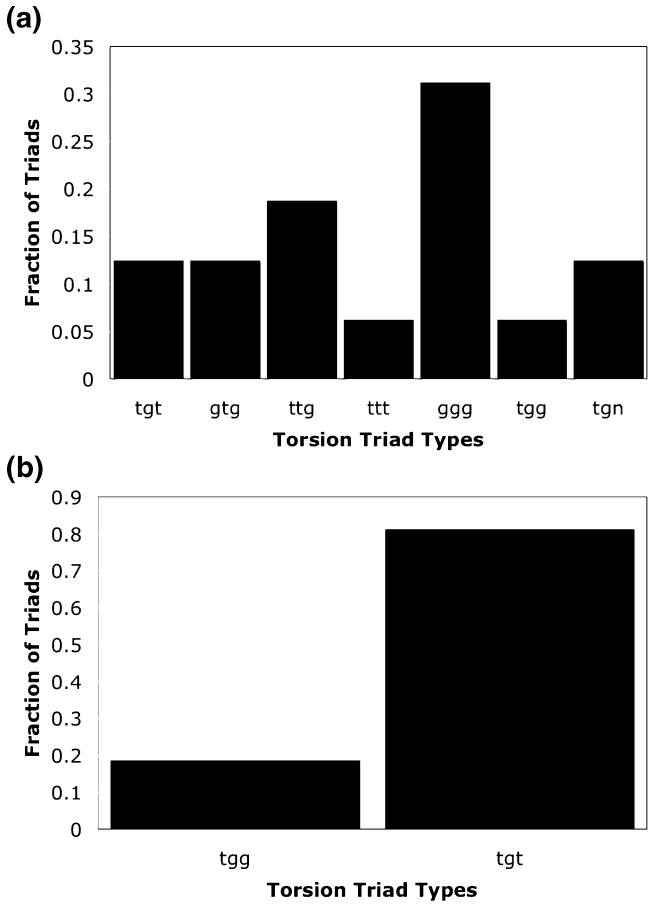

Figure 4. Pair of histograms detailing the population of triad types found in a representative monoglyme system (a) before and (b) after the simulation was performed. In the initial state, a wide variety of triad combinations existed in the system. After the optimization procedure, only two showed appreciable populations, both of which represented low-strain structures as determined by previous work.

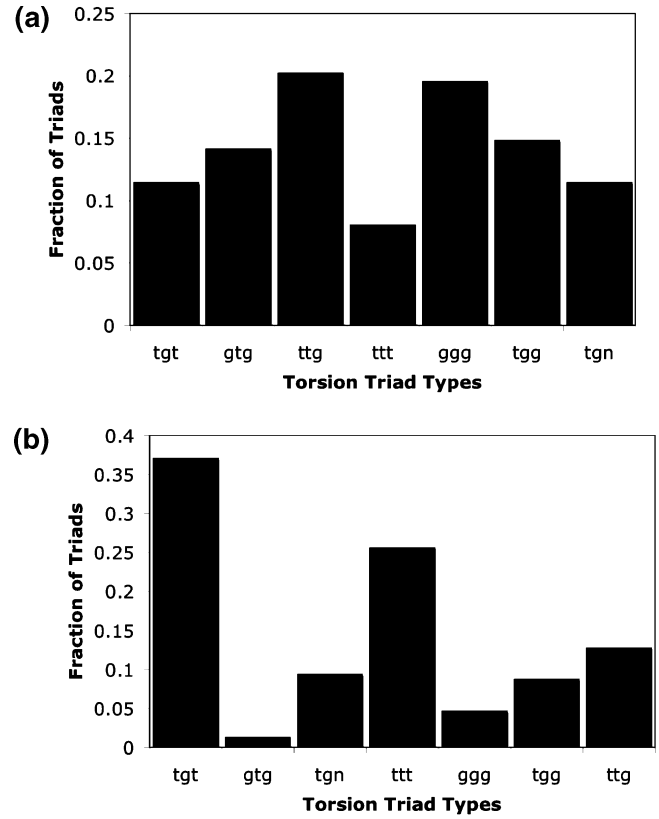

Figure 5. Pair of histograms detailing the population of triad types found in a representative tetraglyme system (a) before and (b) after the simulation was performed. In the initial state, a wide variety of triad combinations existed in the system. After the optimization procedure, the populations shifted. Triad combinations shown to be common in tetraglyme systems increased in population, whereas those rarely represented in previously published studies decreased.

The parameters for argon were taken from the literature,[41] and the simulation was performed using the NAMD programs[42] with a time step of 1 fs and a nonbonded cutoff of 12 Å. Each simulation involved 540 particles randomly placed inside the box and then minimized for 5000 conjugate gradient minimization steps. For the temperature annealing calculations, the volume of a cubic box was fixed at 30 Å per side. The temperature ranged from 25 to 1025 K in 100 K increments with 50-ps simulations at each temperature. After the highest temperature had been reached, the simulation was run for 200 ps and then cooled by reversing the heating schedule. After the system had returned to 25 K, a final equilibration was performed for 50 ps. The final structure and energy were obtained after a 5000-step conjugate gradient minimization. The pressure−temperature annealing simulations started from the same configuration as the corresponding simulated annealing run. They differed in the following ways: During the heating phase, the pressure was fixed at 0.1 bar, and the system was allowed to expand. During the first 50 ps, the system was held at 1025 K, and the pressure remained at 0.1 bar. During the next 100 ps at 1025 K, the system was allowed to expand dramatically, as the pressure was reduced to 0.025 bar. By the end of this period, the box generally expanded to approximately 40 Å on each side. During the final 50 ps, the system was held at 1025 K. During the rest of the cooling phase, the pressure was increased to as much as 1000 bar, until the system returned to its original volume, and then the volume was fixed. The final 50-ps equilibration and 5000-step minimization were then performed, and the final energy and structure were recorded.

3.2. Monoglyme. Monoglyme (Figure 1) is the smallest oligomeric analogue of the polymer polyethylene oxide (PEO), containing a single ethylene oxide repeat unit, capped with methyl and methoxy groups on either end. The simulations were performed using NAMD and a force field previously derived for PEO analogues.[34] Each of the simulations was performed after 120 molecules had been placed in a random orientation and then placed randomly in the box ensuring that no two atoms were closer than 1.9 Å apart. Again, the traditional temperature annealing runs were performed at a fixed volume in a cubic box having sides of length 26.25 Å. The procedure was exactly as described above for argon, with the only differences noted here. During the heating phase of the pressure−temperature annealing procedure, the pressure was set for 0.05 bar, but it was lowered to 0.025 bar to expand the system. The final box size was approximately 110 Å. The system was compressed during the cooling phase with a pressure of as much as 400

bar until the original volume was restored, although as the volume neared its original value, the pressure was slowly reduced to avoid overcompression.

3.3. Tetraglyme. Tetraglyme (Figure 1) is an oligomeric analogue for polyethylene oxide (PEO) containing four repeat units. The simulations were performed using NAMD and the same force field as used for monoglyme and intended for PEO analogues.[34] Each of the simulations was performed after 50 molecules had been placed in a random orientation and then placed randomly in the box ensuring that no two atoms were closer than 1.9 Å. Again, the traditional temperature annealing runs were performed at a fixed volume in a cubic box having sides of length 26.5 Å. The procedure was exactly as described above, with the only differences described here. During the heating phase of the pressure−temperature annealing procedure, the pressure was set to 0.1 bar, but it was lowered to 0.025 bar to expand the system. The final box size was approximately 100 Å. The system was compressed during the cooling phase with a pressure of 500 bar until the original volume was restored, although as the volume neared its original value, the pressure was slowly reduced to avoid overcompression.

3.4. Procedure. For each of the systems described above, a number of random structures were generated. For the Lennard-Jones system, 50 random configurations were generated. For the polymer models, 25 configurations were generated. For each of these random structures, both temperature annealing and pressure annealing simulations were performed, and the final energies and structures were recorded.

4. Results and Discussion

The data collected in the simulations described in the previous section demonstrate that the use of pressure as a coordinate in optimization simulations significantly affects the energies of the structures obtained. For 52% of the Lennard-Jones simulations, 84% of the monoglyme simulations, and 68% of the tetraglyme simulations, the energy of the state produced by the pressure annealing procedure was lower than that produced from the same starting structure but by following the traditional temperature annealing procedure. Each of the final states was characterized by a variety of structural measurements including radial distribution functions, radii of gyration, mean square end-to-end differences, and characteristic ratios. Torsion triad analysis was also performed for the polymer model systems. Each of the structures produced structural data consistent with published results.[34−36] Following is a more detailed look at the results, along with a discussion of their significance.

4.1. Energy Results. The final energies from each simulation started from a random structure are listed in Tables 1−3. They reveal two interesting features. First, of the 50 simulations performed on the Lennard-Jones system, only 52% of the random structures yielded a lower energy during the pressure annealing simulations. This indicates that pressure does not have a significant effect on the results of the simulation, as the results are randomly distributed within the two simulation techniques. For the other two types of simulations, the effect is more pronounced. For the monoglyme simulations, the pressure annealing method generated a lower energy 84% of the time, and for the tetraglyme simulations, pressure annealing generated a lower energy 68% of the time. Whereas the Lennard-Jones system shows no apparent advantage of pressure annealing, the bulkier models adopt structures of noticeably lower energies when the pressure annealing method is used.

4.1.1. Bayesian Statistical Analysis. To answer more precisely the question of whether simulations using pressure plus temperature annealing give lower-energy structures than simulations using temperature annealing alone, we appeal to Bayesian statistics. For similar questions that have a binary success/fail answer, the binomial distribution has been used. This discrete function

$$f(\theta;N,k) = \binom{N}{k}\theta^k(1 - \theta)^{N-k}$$

defines the probability for k successes to occur in a data set of N trials, where the probability of success is θ for each individual trial.[43] In the classic example of a coin toss, we can define a "success" as the coin landing on heads, and we generally believe $\theta = 0.5$. In our present work, we can define a success as a trial where the pressure annealing simulation provides a lower energy than the corresponding temperature annealing simulation. In our work, however, we are interested in estimating the value of the unknown probability θ. This value indicates the fraction of times we would expect pressure annealing to outperform temperature annealing given a random starting structure.

An estimation of θ can be readily achieved using Bayesian statistical analysis.[44] Even more usefully, Bayesian analysis allows the "credibility" that θ lies within a given interval to be estimated. This is accomplished by application of Bayes' theorem. This theorem links two complimentary conditional probabilities together

$$P(\theta|D) \propto P(D|\theta)\,P(\theta)$$

In the language of Bayesian statistical analysis, $P(\theta)$ is called the prior distribution; $P(D|\theta)$ is the conditional probability that our data, D, should be observed given any probability θ; and $P(\theta|D)$ is called the posterior distribution and represents our revised beliefs about the problem given both our prior opinion and our observed data. Thus, we can estimate the conditional probability, $P(\theta|D)$, if both $P(\theta)$ and $P(D|\theta)$ are known or can at least be plausibly represented.

We use the previously introduced binomial distribution to represent the conditional probability of our data (given θ). We choose the beta distribution[43]

$$g(\theta;\alpha,\beta) = \left(\frac{\Gamma(\alpha + \beta)}{\Gamma(\alpha)\,\Gamma(\beta)}\right)\theta^{\alpha-1}(1 - \theta)^{\beta-1}$$

to represent our prior distribution. The beta distribution is a continuous-variable analogue of the binomial distribution (as α and β can take real values) and is chosen because it is a conjugate prior distribution. A prior distribution is conjugate when the chosen prior and conditional probabilities combine to give a posterior distribution with the same form as the prior distribution.

We analyze our simulations using four distinct choices for the prior distribution. In the first case, an "unbiased" distribution, we select $\alpha = 1$ and $\beta = 1$. This choice means that any choice of θ has equal probability. In the second case, an "even" distribution, we select $\alpha = 25$ and $\beta = 25$. This choice gives almost zero probabilities for values of θ far from 0.5, but relatively high probabilities in that region. The other two choices give high probabilities for choices of θ higher than 0.5 (the "over" distribution) and for choices of θ lower than 0.5 (the "under" distribution). These correspond to functions that select $\alpha = 25$ and $\beta = 5$ and $\alpha = 5$ and $\beta = 25$, respectively.

Thus we model our posterior distribution with the following functional form

$$P(\theta|D) = Cf(\theta;N,k)\, g(\theta;\alpha,\beta) = \left(\frac{\Gamma(N+\alpha+\beta-1)}{\Gamma(\alpha+k)\,\Gamma(N-k+\beta)}\right)\theta^{k+\alpha-1}(1-\theta)^{N-k+\beta-1}$$

and we can determine the credibility that $\theta > 0.5$ (which is expected if the pressure annealing technique is a better alternative than temperature annealing) by finding the value of the integral

$$I = \int_{0.5}^{1} P(\theta|D)\, \mathrm{d}\theta$$

The results of this analysis are given in Table 4.

The results are consistent with our analysis in the previous section. The control test involving the Lennard-Jones simulations indicates a minimal advantage to using pressure annealing, whereas both the monoglyme and tetraglyme test cases indicate a particularly clear advantage to pressure annealing. Even when analyzed using a prior distribution that is strongly biased against the favorability of pressure annealing, the credibility for the interval $0.5 < \theta < 1$ is still 34% for monoglyme.

4.1.2. Implications of Statistical Analysis. The results of the previous section support the hypothesis that the expansion of the system under low pressure, followed by compression, allows the system to pack more efficiently. The point particles represented in the Lennard-Jones simulations have little packing complexity, whereas each of the polymer models has not only intermolecular packing concerns but also intramolecular packing to take into account. Expansion frees the system to perform intramolecular reorganization, and compression helps find an optimal intermolecular arrangement. Based on these results, using pressure as an optimization parameter seems to benefit the search for low-energy structures of hindered systems.

4.2. Structural Results. It is important to verify that each of the states generated correspond to relevant structures that have been previously observed. Therefore, each of the states generated by these methods was characterized in a variety of ways and checked against previous results. For the Lennard-Jones simulations, pair radial distributions functions were generated and compared with those of similar systems. For the polymer models, radii of gyration and mean square end-to-end distances were calculated and compared. These values allowed calculation of the system's characteristic ratio, an additional check. Finally, the torsion angles along the backbone of the polymer models were analyzed using a technique called torsional triad analysis, which can be further compared with previous results. In general, the states generated during the course of this work match previous results well and imply that calculated average structures are similar to those reported previously.[34−36]

4.2.1. Radial Distribution Functions. The radial distribution function counts the density of atom pairs within a certain distance window from each other, relative to the density of a bulk fluid. The radial distribution function can be represented as

$$g(r) = \frac{V}{N^2}\left\langle \sum_i \sum_{j\neq i} \delta(r - r_{ij}) \right\rangle^2$$

where r is the distance between atom pairs, V is the volume, N is the number of particles in the system, and r_{ij} is the distance between a specific atom pair. In Figure 3, the pair-radial distribution function representing the lowest-energy Lennard-Jones system found in this work is shown. This radial distribution function is typical of fluids with a relatively high degree of order. It is zero until approximately 3.9 Å (the distance of closest approach allowed by the interatomic potential function). The high initial peak results from nearest-neighbor contacts at a distance approximately equal to the sum of Lennard-Jones radii for the particles. More distant, less distinct peaks have a similar interpretation. This figure is typical of the results generated in this work for these systems and is a good comparison with previous work performed on like systems.[41]

4.2.2. Radius of Gyration, Mean Square End-to-End Distance, and Characteristic Ratio. The remaining tests in this section were used to characterize the structures of the two oligomeric systems studied here. The three measurements described in this section are interrelated and measure bulk properties of the molecules under study; specifically, they describe the arrangement of the atoms in relation to the center of mass or the ends of the molecule. The first measurement, the radius of gyration, is defined as[45]

$$S^2 = \frac{1}{N}\sum_{k=1}^{N} \|\mathbf{r}_k - r_{\mathrm{mean}}\|^2$$

Table 4. Results of the Bayesian Statistical Analysis To Assess the Viability of Pressure−Temperature Annealing To Complement Temperature Annealing When Searching for Low-Energy Structures of Constrained Systems[a]

	Lennard-Jones systems ($N = 50$, $k = 26$)	monoglyme systems ($N = 25$, $k = 21$)	tetraglyme systems ($N = 25$, $k = 17$)
unbiased: $\alpha = 1$, $\beta = 1$	0.610	0.9997	0.962
even: $\alpha = 25$, $\beta = 25$	0.580	0.976	0.852
over: $\alpha = 25$, $\beta = 5$	0.994	0.99999999	0.99997
under: $\alpha = 5$, $\beta = 25$	0.021	0.342	0.067

[a] Contents of the table indicate the credibility that $\theta > 0.5$.

Table 5. Radius of Gyration ($\langle S^2 \rangle$), Mean Square End-to-End Distance ($\langle R^2 \rangle$), and Characteristic Ratio (C_n) for Each of the Runs Involving Monoglyme[a]

	temperature annealing			pressure−temperature annealing		
system	$\langle S^2 \rangle$ (Å^2)	$\langle R^2 \rangle$ (Å^2)	C_n	$\langle S^2 \rangle$ (Å^2)	$\langle R^2 \rangle$ (Å^2)	C_n
1	12.64294	29.95462	4.131672	12.63144	30.05138	4.145018
2	12.642	29.25339	4.03495	12.63144	30.05138	4.145018
3	12.68264	29.04504	4.006212	12.63144	30.05138	4.145018
4	12.62215	29.71162	4.098154	12.63144	30.05138	4.145018
5	12.65295	29.33647	4.04641	12.63144	30.05138	4.145018
6	12.67993	29.25582	4.035286	12.63144	30.05138	4.145018
7	12.64122	29.19647	4.027099	12.63144	30.05138	4.145018
8	12.6627	29.50217	4.069265	12.63144	30.05138	4.145018
9	12.73361	29.27499	4.03793	12.63144	30.05138	4.145018
10	12.64571	29.5682	4.078372	12.63144	30.05138	4.145018
11	12.64617	29.42254	4.058281	12.65642	29.56905	4.07849
12	12.64617	29.42254	4.058281	12.69759	29.81467	4.112368
13	12.64617	29.42254	4.058281	12.67364	29.93132	4.128458
14	12.64617	29.42254	4.058281	12.66215	29.8647	4.119269
15	12.64617	29.42254	4.058281	12.64929	29.47143	4.065025
16	12.64617	29.42254	4.058281	12.63597	29.97904	4.13504
17	12.64617	29.42254	4.058281	12.69603	29.2091	4.028841
18	12.64617	29.42254	4.058281	12.72194	29.59777	4.082451
19	12.64617	29.42254	4.058281	12.67191	29.86696	4.119581
20	12.64617	29.42254	4.058281	12.64283	29.80467	4.110989
21	12.68304	29.33573	4.046308	12.67301	29.23696	4.032684
22	12.65052	29.78779	4.108661	12.68439	29.82505	4.1138
23	12.62334	29.23872	4.032927	12.72182	30.34298	4.185239
24	12.66012	30.01462	4.139948	12.6111	30.06649	4.147102
25	12.65458	29.26337	4.036327	12.61566	29.70253	4.096901

[a] Structural data compiled from the final structures from each run for both the temperature annealing and pressure−temperature annealing simulations.

Table 6. Radius of Gyration ($\langle S^2 \rangle$), Mean Square End-to-End Distance ($\langle R^2 \rangle$), and Characteristic Ratio (C_n) for Each of the Runs Involving Tetraglyme[a]

	temperature annealing			pressure−temperature annealing		
system	$\langle S^2 \rangle$ (Å^2)	$\langle R^2 \rangle$ (Å^2)	C_n	$\langle S^2 \rangle$ (Å^2)	$\langle R^2 \rangle$ (Å^2)	C_n
1	12.95637	124.1425	4.280776	12.76893	129.1815	4.454534
2	12.88302	118.7149	4.093617	12.89379	130.1666	4.488503
3	12.90877	132.4862	4.56849	12.898	129.0914	4.451428
4	12.86335	129.6162	4.469524	12.976	133.3446	4.59809
5	12.92801	124.0264	4.276772	12.94306	123.1806	4.247607
6	12.95901	119.7428	4.129062	12.9213	138.1344	4.763255
7	12.86378	130.5432	4.50149	12.90611	128.7697	4.440334
8	12.82505	135.4648	4.6712	12.91239	132.9224	4.583531
9	12.90405	132.8103	4.579666	12.84688	125.0199	4.311031
10	12.90094	116.7909	4.027272	12.91853	128.7571	4.4399
11	12.93324	124.7005	4.300017	12.86183	128.4394	4.428945
12	12.79128	133.3978	4.599924	12.93111	134.0236	4.621503
13	12.89667	117.9688	4.06789	13.00522	138.3031	4.769072
14	12.87578	119.3006	4.113814	12.86455	125.1847	4.316714
15	12.9339	123.0498	4.243097	12.81507	139.8334	4.821841
16	12.9282	128.7497	4.439645	12.84843	134.7138	4.645303
17	12.84452	135.5878	4.675441	12.95821	140.6227	4.849059
18	12.98611	130.0819	4.485583	12.9139	136.3271	4.700934
19	12.87325	129.7357	4.473645	12.86061	141.1341	4.866693
20	12.96661	131.3619	4.529721	12.96339	148.0451	5.105003
21	12.92065	131.6316	4.539021	12.83847	131.696	4.541241
22	12.95	118.5199	4.086893	12.88816	134.5525	4.639741
23	12.85471	127.7803	4.406217	12.94454	125.419	4.324793
24	12.92728	134.0905	4.62381	13.00921	137.0178	4.724752
25	12.90026	110.0911	3.796245	12.95532	129.1935	4.454948

[a] Structural data compiled from the final structures from each run for both the temperature annealing and pressure−temperature annealing simulations.

and measures the extent to which the polymer's mass deviates from its center of gravity. It gives some indication as to how tightly the polymer arranges itself. Of course, the chemical and physical nature of the polymer determines this value, which varies according to the physical conditions in which the polymer exists. However, previous studies showed that, for tetraglyme, the value is approximately 20 Å^2.[35] Published data for monoglyme are unavailable. The mean square end-to-end distance, R^2, of the polymer is quite easily defined. It is simply the distance from one end of the polymer

to the other, squared,[45] and then averaged over time and the number of polymer molecules in the sample. This gives a good measure of whether the polymer is stretched (or coiled) or compact. Again, this measurement depends directly on the polymer in question and the physical conditions in which it exists. For tetraglyme, a value of approximately 140 Å has been reported. Finally, the characteristic ratio[45] is an important measurement, because it relates the radius of gyration in a unitless form that is easier to compare between oligomers of different lengths. Additionally, according to theoretical calculations, the value has significance in determining the amount of flexibility the polymer has. For a freely jointed polymer of infinite length, the characteristic ratio should be 1. In the freely rotating chain model, the value can be used to determine the bond angle.[45] The characteristic ratio is defined as

$$C_n = \frac{R^2}{nl^2}$$

where n is the number of backbone bonds in the oligomer and l is an average bond distance in the polymer system (approximately 1.5 Å for the glymes, based on published geometries in ref 33, for example). C_n for tetraglyme has been reported to be 4.9.[34,35] Tables 5 and 6 list the radii of gyration, mean squared end-to-end distances, and characteristic ratios for the oligomer simulations performed here. All calculated values for the mean squared end-to-end distances for tetraglyme are within 30% of the previously reported ensemble average and values obtained using pressure annealing are considerably closer, within 9%. In addition, most calculated values of the characteristic ratio are within a few tenths of an angstrom, with a maximum deviation of −1.1 Å (22%) from the published, ensemble-average value for temperature annealing and 13% (0.65 Å) for pressure annealing. The radii of gyration are uniformly lower than previously reported, and perhaps indicate a difference due to temperature effects or the fact that these values represent a single minimized structure, whereas the published values are taken from an ensemble average at 300 K.

4.2.3. Torsional Triad Population. This measurement[34−36] is specific to oligomers or polymers, as it can be defined only for a given backbone atom sequence of three bonds. Triad analysis for PEO requires measuring a series of three torsion angles each time they occur, classifying the conformations as trans (labeled t, encompassing angles from 120° to 240°), gauche (labeled g, encompassing angles from 0° to 120°), or gauche minus (labeled n, encompassing angles from 240° to 360°). The triads are characterized by three letters. The combination ttt, for example, indicates that all three angles in the triad are trans. Finally, the number of times each combination occurs is counted and used to generate the figures described below. Figure 1 shows that monoglyme contains only a single conformational triad defined by torsional angles around bonds labeled 2−3, 3−4, and 4−5. Tetraglyme, on the other hand, contains four triads in each molecule. Figure 4 shows how the distribution of triads changed between the random initial state and the final state for the monoglyme simulation that produced the lowest energy. Initially, the triad distribution was random, containing a wide variety of triad combinations. After the optimization was performed, only two types of triads predominated, corresponding to low-energy states of each individual strand. The tgt triad dominated, as expected because it is known to represent the dominant triad in glyme systems.[34−36] A similar situation occurred in the tetraglyme simulation that yielded the lowest energy, depicted in Figure 5. Again, the initial state contained a variety of traid combinations, but after the simulation was performed, more dominant triads emerged. Two triads in particular, tgt and ttt, each became more populated, which is consistent with previously reported results.[34−36] Also, states such as gtg that were only minimally populated in previous works dropped in population considerably.[34−36]

5. Conclusions

We have shown that pressure annealing (pressure−temperature annealing) can help to find low-energy structures of systems complicated by steric hindrance. We hypothesize that this is due to the effect that lowered density (due to the lowered pressure) has on a bulky molecule's ability to rearrange itself. Pressure annealing was tested here by allowing such conditions to be realized. Additionally, the final compression phase helps to pack the well-folded molecules onto each other. We showed that bulky molecules gave a lower energy nearly 70% of the time (and as high as 80% in monoglyme) during pressure−temperature annealing simulations when compared to conventional simulated annealing. In contrast, for the simpler Lennard-Jones model, pressure−temperature annealing performed better only 52% of the time and thus gave no appreciable benefits. The conventional simulated annealing simulations and the pressure annealing simulations executed identical numbers of MD and minimization steps and so took essentially equal amounts of time to complete, which demonstrates a further advantage for the pressure annealing simulations.

For the systems studied, the radial distribution functions, radii of gyration, mean squared end-to-end distances, characteristic ratios, and torsion triad populations generated by the method compare well with published results. Pressure annealing shows promise and should be further studied through application to other systems. In particular, applications of the technique to studying the low-energy conformations of longer oligomers, peptides, and small proteins might be pursued. This method, especially in simulations with explicit solvent, would seem to be a very promising approach.

Finally, different heating and cooling schedules can have a significant effect on the results of temperature annealing studies, and an extensive literature exists discussing various possible heating/cooling schedules. Although we selected one particular cooling (and expansion/compression) schedule simply to illustrate the utility of pressure annealing, many others exist, and their effects should be investigated systematically in subsequent work. Another avenue that deserves further exploration includes incorporating the ideas of this work into the replica-exchange framework. Exchanging replicas at different pressures as well as different tempera-

tures could yield a robust optimization technique, particularly in systems containing explicit solvent.

Acknowledgment. We are grateful for supercomputer time from the NSF/NRAC, through Award MCA96-N019, and from the Oklahoma Supercomputing Center for Education and Research (OSCER). Mr. Kevin Raymond first used this method for equilibrating simulations of long oligomers. We acknowledge helpful conversations with Prof. Kieran Mullen during the writing of this article.

References

(1) Malandro, D. L.; Lacks, D. J. Volume dependance of potential energy landscapes in glasses. *J. Chem. Phys.* **1997**, *107*, 5804–5810.

(2) Allen, M. P.; Tildesley, D. J. *Computer Simulations of Liquids*; Clarendon Press: Oxford, U.K., 1987.

(3) Tsallis, C.; Stariolo, D. A. Generalized simulated annealing. *Physica A* **1996**, *233*, 395–406.

(4) Kirkpatrick, S.; Gelatt, C. D.; Vecchi, M. P. Optimization by Simulated Annealing. *Science* **1983**, *220*, 671–680.

(5) Cantoni, O. In *Lecture Notes in Mathematics/Seminaire de Probabilities*; Azema, J., Emery, M., Ledoux, M., Yor, M., Eds.; Springer-Verlag: Berlin, 1999; Vol. 33, pp 69−119.

(6) Nilges, M.; Gronenborn, A. M.; Brunger, A. T.; Clore, G. M. Determination of three-dimensional structures of proteins by simulated annealing with interproton distance restraints. Application to crambin, potato carboxypeptidase inhibitor and barley serine proteinase inhibitor 2. *Protein Eng.* **1988**, *2*, 27–38.

(7) Hohl, D.; Jones, R. O.; Car, R.; Parrinello, M. Structure of sulfur clusters using simulated annealing: S2 to S13. *J. Chem. Phys.* **1988**, *89*, 6823–6835.

(8) Wilson, S. R.; Cui, W. L. Applications of simulated annealing to peptides. *Biopolymers* **1990**, *29*, 225–35.

(9) Cohn, H.; Fielding, M. Simulated annealing: Searching for an optimal temperature schedule. *SIAM J. Optim.* **1999**, *9*, 779–802.

(10) Sugita, Y.; Okamoto, Y. Replica-exchange molecular dynamics method for protein folding. *Chem. Phys. Lett.* **1999**, *314*, 141–151.

(11) Koehl, P.; Delarue, M. Mean-field minimization methods for biological macromolecules. *Curr. Opin. Struct. Biol.* **1996**, *6*, 222–6.

(12) Ladd, M. F. C.; Palmer, R. A. *Structure Determination by X-Ray Crystallography*; Springer: New York, 1994.

(13) Cui, F. Distance-based NMR Structure Determination and Refinement. Ph.D. Thesis, Iowa State University, Ames, IA, 2006.

(14) Townes, C. H.; Schawlow, A. L. *Microwave Spectroscopy*; Dover: Mineola, NY, 1975.

(15) Pulay, P.; Fogarasi, G. Geometry optimization in redundant internal coordinates. *J. Chem. Phys.* **1992**, *96*, 2856.

(16) Allinger, N. L.; Yuh, Y. H.; Lii, J.-H. Molecular Mechanics. The MM3 Force Field for Hydrocarbons. 1. *J. Am. Chem. Soc.* **1989**, *111*, 8551.

(17) Cornell, W. D.; Cieplak, P.; Bayly, C. I.; Gould, I. R.; Merz, K. M.; Ferguson, D. M.; Spellmeyer, D. C.; Fox, T.; Caldwell, J. W.; Kollman, P. A. A Second Generation Force Field for the Simulation of Proteins, Nucleic Acids, and Organic Molecules. *J. Am. Chem. Soc.* **1995**, *117*, 5179–5197.

(18) Press, W. H.; Flannery, B. P.; Teukolsky, S. A.; Vetterling, W. T. *Numerical Recipes: The Art of Scientific Computing*; Cambridge University Press: New York, 1986.

(19) Elber, R.; Karplus, M. Enhanced sampling in molecular dynamics: Use of the time-dependent Hartree approximation for a simulation of carbon monoxide diffusion through myoglobin. *J. Am. Chem. Soc.* **1990**, *112*, 9161–75.

(20) Gerber, R. B.; Buch, V.; Ratner, M. A. Time-Dependent Self-Consistent Field Approximation for Intramolecular Energy Transfer. 1. Formulation and Application to Dissociation of van der Waals Molecules. *J. Chem. Phys.* **1982**, *77*, 3022–3030.

(21) Simmerling, C.; Miller, J. L.; Kollman, P. A. Combined Locally Enhanced Sampling and Particle Mesh Ewald as a Strategy To Locate the Experimental Structure of a Nonhelical Nucleic Acid. *J. Am. Chem. Soc.* **1998**, *120*, 7149–7155.

(22) Hixson, C. A.; Chen, J.; Huang, Z. N.; Wheeler, R. A. New perspectives on multiple-copy, mean-field molecular dynamics methods. *J. Mol. Graph. Model.* **2004**, *22*, 349–357.

(23) Simmerling, C.; Lee, M. R.; Ortiz, A. R.; Kolinski, A.; Skolnick, J.; Kollman, P. A. Combining MONSSTER and LES/PME to Predict Protein Structure from Amino Acid Sequence: Application to the Small Protein CMTI-1. *J. Am. Chem. Soc.* **2000**, *122*, 8392–8402.

(24) Roitberg, A.; Elber, R. Modeling side chains in peptides and proteins: Application of the locally enhanced sampling and the simulated annealing methods to find minimum energy conformations. *J. Chem. Phys.* **1991**, *95*, 9277–87.

(25) Zheng, Q.; Rosenfeld, R.; DeLisi, C.; Kyle, D. J. Multiple copy sampling in protein loop modeling: Computational efficiency and sensitivity to dihedral angle perturbations. *Protein Sci.* **1994**, *3*, 493–506.

(26) Stultz, C. M.; Karplus, M. On the potential surface of the locally enhanced sampling approximation. *J. Chem. Phys.* **1998**, *109*, 8809–8815.

(27) Wickstrom, L.; Okur, A.; Song, K.; Hornak, V.; Raleigh, D. P.; Simmerling, C. L. The unfolded state of the villin headpiece helical subdomain: Computational studies of the role of locally stabilized structure. *J. Mol. Biol.* **2006**, *360*, 1094–1107.

(28) Larios, E.; Pitera, J. W.; Swope, W. C.; Gruebele, M. Correlation of early orientational order of engineered λ_{6-85} structure with kinetics and thermodynamics. *Chem. Phys.* **2006**, *323*, 45–53.

(29) Gnanakaran, S.; Nussinov, R.; Garcia, A. E. Atomic-level description of amyloid β-dimer formation. *J. Am. Chem. Soc.* **2006**, *128*, 2158–2159.

(30) Furlan, S.; La Penna, G.; Perico, A.; Cesaro, A. Conformational Dynamics of Hyaluronan Oligomers in Solution. 3. Molecular Dynamics from Monte Carlo Replica Exchange Simulations and Mode Coupling Diffusion Theory. *Macromolecules* **2004**, *37*, 6197–6209.

(31) Sikorski, A. Properties of Star-Branched Polymer Chains. Application of the Replica Exchange Monte Carlo Method. *Macromolecules* **2002**, *35*, 7132–7137.

(32) Yamada, Y.; Udea, Y.; Kataoka, Y. Replica exchange Monte Carlo simulations for folding of di-block polyampholyte. *J. Comput. Chem. Jpn.* **2005**, *4*, 127–130.

(33) Liboff, R. L. In *Kinetic Theory: Classical, Quantum, and Relativistic Descriptions*. Wiley: New York, 1998.

(34) Dong, H.; Hyun, J.-K.; Durham, C.; Wheeler, R. A. Molecular dynamics simulations and structural comparisons of amorphous polyethylene oxide and polyethylenimine models. *Polymers* **2001**, *42*, 7809–7817.

(35) Dong, H.; Hyun, J.-K.; Rhodes, C. P.; Frech, R.; Wheeler, R. A. Molecular Dynamics Simulations and Vibrational Spectroscopic Studies of Local Structure in Tetraglyme: Sodium Triflate Solutions. *J. Phys. Chem. B* **2002**, *106*, 4878–4885.

(36) Smith, G. D.; Yoon, D. Y.; Jaffe, R. L.; Colby, R. H.; Krishnamoorti, R.; Fetters, L. J. Conformations and Structures of Polyoxyethlyene melts from molecular dynamics simulations and small-angle neutron scattering experiments. *Macromolecules* **1996**, *29*, 3462–3469.

(37) Dias, F. B.; Lambertus, P.; Veldhuis, J. B. J. Trends in polymer electrolytes for secondary lithium batteries. *J. Power Sources* **2000**, *88*, 169–191.

(38) Tarascon, J. M.; Gozdz, A. S.; Schmutz, C.; Shokochi, F.; Warren, P. C. Performance of Bellcore's plastic rechargable Li-ion batteries. *Solid State Ionics* **1996**, *86*−*88*, 49–54.

(39) Hajek, B. Cooling schedules for optimal annealing. *Math. Oper. Res.* **1988**, *13*, 311–329.

(40) McQuarrie, D. A. *Statistical Mechanics*; University Science Books: Sausalito, CA, 2000.

(41) Hixson, C. A.; Wheeler, R. A. Practical multiple-copy methods for sampling classical statistical mechanical ensembles. *Chem. Phys. Lett.* **2004**, *386*, 330–335.

(42) Phillips, J. C.; Braun, R.; Wang, W.; Gumbart, J.; Tajkhorshid, E.; Villa, E.; Chipot, C.; Skeel, R. D.; Kale, L.; Schulten, K. Scalable molecular dynamics with NAMD. *J. Comput. Chem.* **2005**, *26*, 1781–1802.

(43) Stuart, A.; Ord, K. *Kendall's Advanced Theory of Statistics*, 6th ed.; Oxford University Press: New York, 1994; Vol. 1.

(44) Lee, P. M. *Bayesian Statistics: An Introduction*; Oxford University Press: New York, 2004.

(45) Flory, P. J. *Statistical Mechanics of Chain Molecules*; Interscience Publishers: New York, 1969.

CT800451C